Evolutionary optimization of the short-circuit current enhancement in organic solar cells by nanostructured electrodes

(iD) Ping Bai, (iD) Mohamed S. Abdelkhalik, (iD) Diogo G. A. Castanheira, et al.

View Online   **Export Citation**   **CrossMark**

ARTICLES YOU MAY BE INTERESTED IN

Evolutionary optimization of the short-circuit current enhancement in organic solar cells by nanostructured electrodes

Ping Bai,[1,a)] (ID) Mohamed S. Abdelkhalik,[1] (ID) Diogo G. A. Castanheira,[1] (ID) and Jaime Gómez Rivas[1,2,b)] (ID)

AFFILIATIONS

[1]Department of Applied Physics and Science Education, and Eindhoven Hendrik Casimir institute, Eindhoven University of Technology, P.O. Box 513, 5600 MB Eindhoven, The Netherlands
[2]Institute for Complex Molecular Systems, Laboratory of Macromolecular and Organic Chemistry, Eindhoven University of Technology, 5600 MB Eindhoven, The Netherlands

[a)]Author to whom correspondence should be addressed: p.bai@tue.nl
[b)]Electronic mail: j.gomez.rivas@tue.nl

ABSTRACT

Using a particle swarm optimization algorithm (a population-based stochastic optimization technique) combined with 3D finite-difference time-domain simulations, we inverse design periodic arrays of metallic nanoparticles on indium-tin-oxide electrodes and nanoholes in metallic thin films working as electrodes in P3HT (Poly(3-hexylthiophene-2,5-diyl)):PCBM ([6,6]-Phenyl C61 butyric acid methyl ester) organic solar cells to achieve the maximum short-circuit currents (J_{sc}). Nanohole-array electrodes have large optical losses, leading to a net reduction of J_{sc} compared to a reference solar cell. On the other hand, nanoparticle arrays can lead to a significant enhancement of J_{sc} of up to 20%. Detailed simulations show that this enhancement is caused by the grating coupling of the incident light to surface plasmon polaritons at the interface of the metal electrode and the hole transport layer, leading to the enhancement of the electromagnetic field in the organic blend.

Published under an exclusive license by AIP Publishing. https://doi.org/10.1063/5.0097964

I. INTRODUCTION

Organic solar cells (OSCs) based on bulk heterojunctions are promising candidates for renewable energy sources thanks to their advantages compared to inorganic solar cells, such as low-cost, lightweight, and mechanical flexibility.[1] Significant progress has been made on OSC processing, device configuration, and film morphology to achieve high power-conversion efficiencies (PCEs).[2–4] However, organic materials have several drawbacks that impact the overall performance of solar cells. For example, the relatively low carrier mobilities and short exciton-diffusion lengths lead to typically very thin photo-active layers, of around 100 nm, which limits the light-absorption and the energy conversion efficiencies.[5,6] Many efforts have been made to improve the PCE in OSCs by increasing the short-circuit current (J_{sc}),[7,8] open-circuit voltage (V_{OC}),[9–11] or extending the absorption spectrum.[12] Resonant light trapping in OSCs has attracted much attention in recent years, as it enables thin devices with high optical absorption.[13–15] Light absorption could be improved by implementing metallic nanoparticles or nanohole arrays into solar cell devices. These structures can introduce plasmonic effects, such as localized surface plasmon resonances (LSPRs),[16–20] surface plasmon polaritons (SPPs),[21] and quasi-guided modes into OSCs.[22,23] To introduce resonant structures in OSCs, a comprehensive analysis of their structure is required to optimize the size,[22,24] shape,[25] composition,[26] and lattice constant.[22,27] Besides resonant metallic structures for light absorption, metallic nanomeshes and nanowire networks have been also considered potential alternatives to indium-tin-oxide (ITO) electrodes.[21,28,29]

In this paper, we use evolutionary optimization to explore the potential of plasmonic nanoparticle and nanohole arrays defining the cathode of P3HT:PC$_{61}$BM OSCs to enhance the short-circuit current (J_{sc}) compared to standard devices. Two different OSC architectures are considered: solar cells with periodic aluminum nanoparticles on top of the ITO electrode (nanoparticle array solar cell) and solar cells with nanohole arrays in an aluminum thin film

acting as a conducting semitransparent electrode that replaces the ITO electrode (nanohole-array solar cell). A particle swarm optimization (PSO) algorithm code,[30,31] combined with 3D finite-difference time-domain (FDTD) simulations, is used to determine the nanoparticle or nanohole dimensions and the square lattice constant for the maximum J_{sc} under 1 sun illumination. Our numerical simulations conclude that nanohole-array electrodes always reduce J_{sc} compared to standard devices due to their relative low transmission despite being this transmission enhanced at defined wavelengths due to the excitation of SPPs. On the other hand, the plasmonic resonances of nanoparticle arrays on top of the ITO electrode enhance J_{sc} by 20% in the optimized particle array by confining the electromagnetic field into the organic blend and extending the absorption spectrum of the solar cell.

Plasmonic nanoparticles can be made of a variety of materials, such as gold[32,33] and silver.[34–36] However, the high cost or stability of these materials prevents their use in real applications. Therefore, we will limit our study to aluminum (Al) as an inexpensive and stable material with a good plasmonic response in the visible.[37] Al nanoparticles exhibit not only a resonant enhancement of light scattering and absorption due to plasmonic resonances, but they can act as quenchers of triplet excitons, improving the stability of the device.[38]

Systematic numerical investigations of nanostructured organic solar cells have been done in the past, where the influence on the absorption of the spacing between nanoparticles, the diameter, the position, or the coating is reported. Most of these works rely on parametric sweeps to calculate the absorption enhancement, rather than on evolutionary methods, as the one presented here, to find the parameters of the best performing solar cell.[22,39,40] Recently, a neural network has been used to determine the maximum absorption enhancement of nanostructured OSCs compared to cells with the same thickness but without nanostructures.[41] These calculations found the maximum enhancement for very thin layers of organic materials, which does not ensure maximum J_{sc} under 1-sun illumination. In contrast, we have performed an evolutionary optimization of J_{sc}, providing parameters that can be realized in functional devices. This optimization is limited to square arrays of Al nanoparticles/holes in P3HT:PC$_{61}$BM solar cells. We note that different values of J_{sc} and further improvements can be obtained when considering different materials or array's geometries. These results illustrate the potential of evolutionary simulations for the improvement of OSCs.

This paper is organized as follows. Section II describes the geometries of the nanoparticle and nanohole-array solar cells and illustrate with two examples the effect of nanostructuring the electrode on the absorption of the blend and J_{sc}. In Sec. III, we apply the PSO algorithm to retrieve the parameters of the arrays and the blend thickness giving the maximum enhancement of J_{sc}. Section IV describes the mechanisms leading to this maximum enhancement in the nanoparticle solar cell. Finally, we investigate in Sec. V the oblique angle illumination of the solar cell to retrieve the dispersion in the absorption.

II. DESIGN OF NANOPARTICLE AND NANOHOLE-ARRAY DEVICES

A schematic representation of the investigated standard solar cell device is depicted in Fig. 1(a). This device consists of a 120 nm

thick layer of ITO as a cathode on top of a glass substrate, a ZnO layer for electron transport with a thickness of 40 nm, a blend of P3HT:PC$_{61}$BM defining the bulk heterojunction, a 10 nm MoO$_3$ layer for hole transport, and an Ag layer with a thickness of 100 nm acting as an anode. The complex values of the refractive index of the blend that are used in the simulations are taken from the literature and given in Fig. 1(b) with the dashed curves.[21] The solid curves in this figure are fits to the empirical results satisfying Kramers–Kroning relations.

For the nanoparticle array solar cell, we design a square array of Al nanoparticles on top of the ITO cathode, as depicted in Fig. 1(c), to explore the optical absorption and the J_{sc} enhancement of the solar cell due to the electromagnetic field confinement in the blend. The Al nanoparticles, with diameter d and height h, are arranged in a periodic square array with a lattice constant a, and subsequent layers are conformally deposited on top.

For the nanohole-array solar cell, a square array of nanoholes in an Al thin film simultaneously works as a semi-transparent electrode to replace the ITO and to enhance the field in the blend, as shown schematically in Fig. 1(e) with nanohole diameter d, height h, and lattice constant a. The holes are filled with ZnO obtaining a planar structure. We aim to explore the effect of the nanohole array in the device directly from the J_{sc} enhancement that represents the total contribution of the transmission through the structured electrode and the absorption in the active layer.

The absorbed power per unit volume can be calculated from the simulated electric-field distribution,

$$P_{abs}(x, y, z, \omega) = \frac{1}{2}\varepsilon_0 \omega |E(x, y, z, \omega)|^2 \varepsilon''(\omega), \quad (1)$$

where $E(x, y, z, \omega)$ is the electric field at coordinates x, y, z and at the angular frequency ω, ε'' is the imaginary component of the permittivity of the material at the same coordinates, and ε_0 is the vacuum permittivity. The absorbed power of the organic blend in the solar cell can be calculated as

$$A(\omega) = \frac{1}{P_{source}} \iiint_V P_{abs}(x, y, z, \omega) dx dy dz, \quad (2)$$

where P_{source} is the power of the incident wave and V is the volume occupied by the blend. By assuming an internal conversion efficiency of the organic blend of 100%, i.e., the number of generated electron–hole pairs is equal to the number of absorbed photons, the short-circuit current density of the solar cell can be determined as

$$J_{sc} = \frac{e}{\hbar S} \int_{\omega_1}^{\omega_2} \frac{A(\omega) S_{AM1.5}}{\omega} d\omega, \quad (3)$$

where e is the electron charge, $\hbar$ is Planck's constant, S is the surface area of the device, and $S_{AM1.5}$ is the AM 1.5 solar spectrum. The integral limits are defined by the absorption spectrum of the organic blend, i.e., $\omega_1 = 430$ and $\omega_2 = 1000$ THz, corresponding to wavelengths in the range of 300–700 nm. The simulations are done
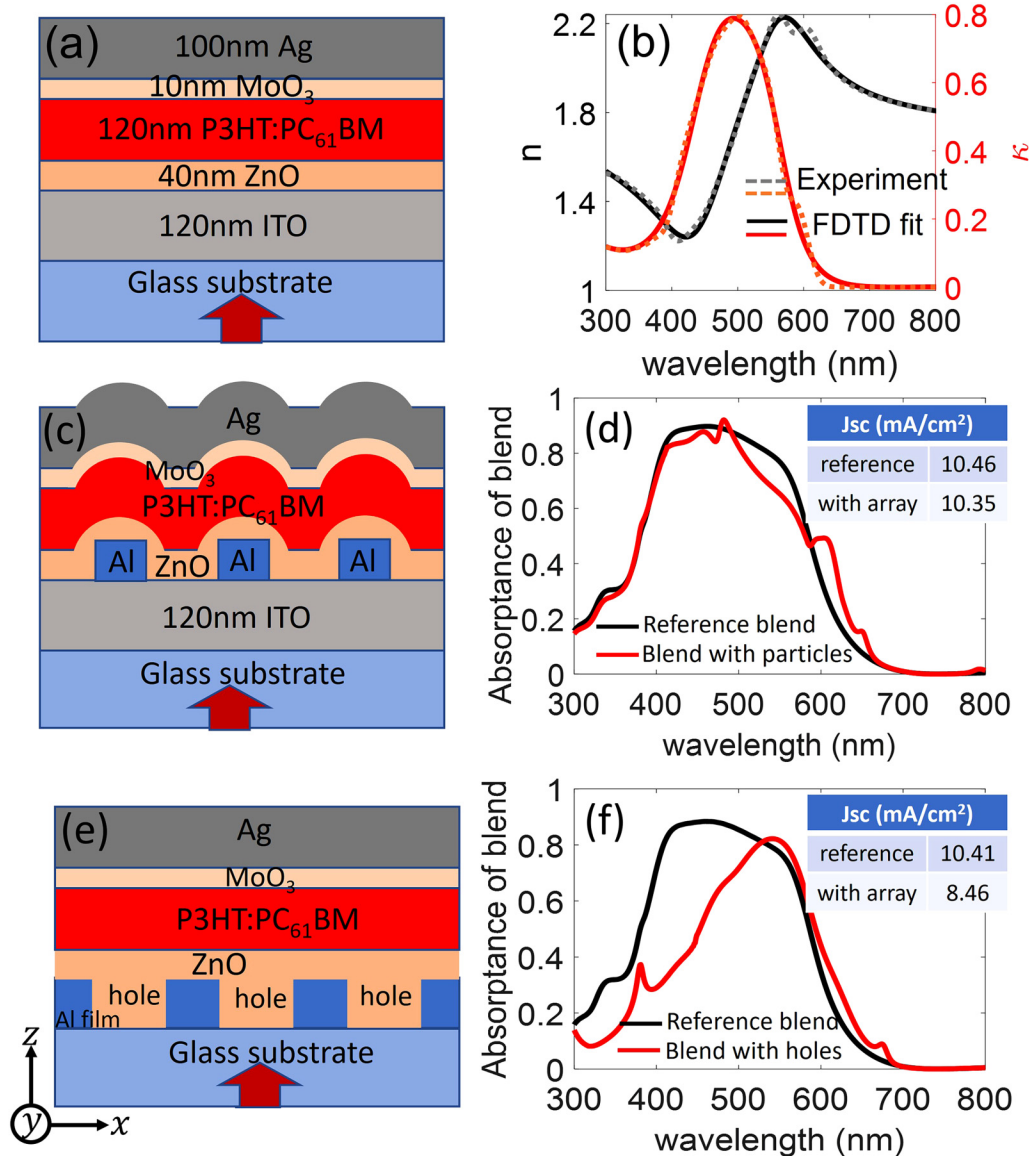
FIG. 1. Schematic cross sections of the layer stack of (a) the reference solar cell, (c) the nanoparticle array solar cell, and (e) the nanohole-array solar cell (e). (b) Experimental refractive index (n) and extinction coefficient (κ) of P3HT:PC$_{61}$BM from Ref. 21 (dashed curves). The fits to the experimental values used for the FDTD simulations are displayed with solid curves. (d) Absorptance of P3HT:PC$_{61}$BM in the reference solar cell (black curve) and in the Al nanoparticle array solar cell (red curve, period $a = 400$, diameter $d = 120$, height $h = 30$, and thickness of blend $t = 120$ nm). The J_{sc} values for both solar cells are given in the inset. (f) Absorptance of P3HT:PC$_{61}$BM in the reference solar cell (black curve) and in a nanohole-array solar cell (red curve, $a = 307$, $d = 257$, $h = 52$, and $t = 123$ nm). The J_{sc} values for both solar cells are given in the inset.

for an incident wave with an amplitude of 1 V/m and a spectral range covering the absorption of the blend.

To illustrate these calculations, we display the absorptance spectrum of the blend in Fig. 1(d) with the red curve for a nanoparticle array solar cell with $d = 120$, $h = 30$, $a = 400$, and a 120 nm thick layer of blend under normal illumination. For comparison, the absorptance spectrum of a standard solar cell with the same thickness of blend is plotted with a black curve. We observe that the absorptance for the nanoparticle array solar cell increases around 600 nm. The absorptance is reduced at shorter wavelengths, with the exception of 480 nm, leading to a net reduction of J_{sc} compared to the reference device as indicated in the inset table of Fig. 1(d).

Similarly, we also calculate the absorptance spectrum of the blend in a nanohole-array solar cell with $d = 257$, $h = 52$, $a = 307$, and 123 nm thickness of blend. The result is displayed in Fig. 1(f) with a red curve, where also, the absorptance of the reference solar cell is plotted for comparison with a black curve. As shown in the inset table of Fig. 1(f) and despite a slight absorptance enhancement that can be observed around the long-wavelength absorption edge of the blend, J_{sc} is greatly reduced compared to the reference due to the lower optical transmittance through the nanohole array.

Although J_{sc} is not improved by introducing the nanoparticle and nanohole arrays into solar cell devices for the above examples, the absorptance spectrum is greatly affected by resonances in these arrays. Next, we optimize the size of nanoparticles and nanoholes, the period of the arrays, and the thickness of the blend to achieve the maximum J_{sc}, which eventually improves J_{sc} of the equivalent devices without structured electrodes. We also analyze the main resonances in the arrays contributing to J_{sc}.

III. PARTICLE SWARM OPTIMIZATION OF THE SHORT-CIRCUIT CURRENT ENHANCEMENT

We incorporate the concept of evolutionary optimization in the form of a PSO algorithm to find the best structural parameters of the nanoparticle and nanohole arrays. This optimization is done by performing 3D-FDTD simulations that yield the highest possible J_{sc} enhancement in OSCs.[30,42] The J_{sc} enhancement is defined as $(J_{sc}/J_{sc}^{ref} - 1) \cdot 100\%$, where J_{sc}^{ref} is the short-circuit current of the reference solar cell with the same thickness of the blend but with a flat ITO electrode instead of the nanohole array or the ITO with a nanoparticle array on top.

The PSO algorithm is used to optimize the J_{sc} enhancement by iteratively improving the parameters. It calculates the J_{sc} enhancement by having a population of solar cell devices that evolve toward the optimum by changing parameters in the search space. Each population change is influenced by its local best-known parameters but is also guided toward the best-known parameters in the search space, which are updated as better parameters are found by other populations. This procedure is expected to move the populations toward the global best set of parameters that correspond to the maximum J_{sc} enhancement.

The diameter d and height h of the cylindrical nanoparticles and nanoholes, the period of the square array a, and the thickness of the blend t for light-harvesting are the parameters that are optimized. For the nanoparticle array solar cells, these parameters are varied in the ranges $d = 20-200$, $h = 20-80$, $a = 200-500$, and $t = 80-140$ nm, while for the nanohole array, solar cells are varied in the ranges $d = 20-500$, $h = 20-150$, $a = 200-600$, and $t = 80-140$ nm. These ranges are limited by realistic values in devices.

Twenty populations are allowed to evolve during 50 generations, as illustrated in Fig. 2(a). This evolution for nanoparticle array solar cells shows an increase in J_{sc} for all the populations as they converge toward the optimum device geometry. This geometry corresponds to the J_{sc} enhancement of ≈20% and parameters $d = 21.4$, $h = 79.7$, $a = 228.6$, and $t = 129.4$ nm. For the nanohole-array solar cells, we always retrieve a reduction of J_{sc} with

a minimum value of 6%, which corresponds to the parameters of $d = 333.5$, $h = 31.2$, $a = 383.5$, and $t = 127.2$ nm.

The evolution of J_{sc} in the 20 populations of nanohole-array solar cells is illustrated in Fig. 2(b). Even though the transmission through a hole array can be enhanced at selected wavelengths by the excitation of surface plasmon polaritons,[43] this enhanced resonant transmission cannot compensate for the high reflection at other wavelengths and the absorption in the metal layer, which give rise to a net reduction of J_{sc}.

The best J_{sc}, mean value of J_{sc}, and standard deviation (SD) for each iteration or generation number are displayed in Figs. 2(c) and 2(d) for the particle and nanohole-array devices, respectively. These figures illustrate the convergence of the maximum J_{sc} and the mean toward the highest J_{sc} and the reduction of the SD during the evolution. To illustrate the changes of the parameters of the population with the highest J_{sc} as a function of the generation number, we show in Fig. 2(e) for the nanoparticle array solar cells and in Fig. 2(f) for the nanohole solar cells period a (black curve), diameter d (red curve), height h (pink curve), and thickness of organic blend t (dark-red curve) for this best population. It is worth noting that all the parameters remain nearly constant after 23 generations with a tolerance of <2 nm compared to the best values at the last generation (50), which illustrates the relative fast convergence of this method.

We also note that the proposed Al nanodisks can be easily fabricated using electron-beam lithography (EBL) or nanoimprint lithography for patterning a photoresist or a sol-gel, followed by electron-beam evaporation for depositing Al nanoparticles with the defined thickness,[42] followed by standard spin coating and evaporation techniques for organic solar cells.[28]

IV. INVESTIGATION OF THE OPTIMUM NANOPARTICLE ARRAY DEVICE

Based on the results of the PSO algorithm, J_{sc} can be significantly enhanced by a nanoparticle array on top of ITO. In this section, we describe the mechanisms responsible for this enhancement. The refractive index n and the extinction coefficient k of the different materials forming the solar cell are shown in Fig. S1 of the supplementary material. Besides the organic blend and the Ag anode, the other materials exhibit almost no absorption in the visible, with the absorption increasing in the UV. Therefore, mainly, the organic blend (donor) absorbs photons under sun light illumination, forming the excitons that have to be dissociated at the interface between the donor and the acceptor. Electrons are collected at the transparent ITO cathode through the electron transport layer (ZnO), while holes are collected at the Ag anode through the hole transport layer (MoO$_3$).

Figure 3(a) shows the absorptance spectrum calculated in the volume occupied by the organic blend in the device with the optimum nanoparticle array for a maximum J_{sc} (black curve). This spectrum is compared to the absorptance of the blend in a standard (reference) device [dashed curve in Fig. 3(a)]. The absorptance is enhanced by the nanoparticle array over the full visible spectrum, being reduced at short wavelengths (<360 nm). The red curve in Fig. 3(a) represents the absorption enhancement in the organic blend by the nanoparticle array, calculated as the ratio between the
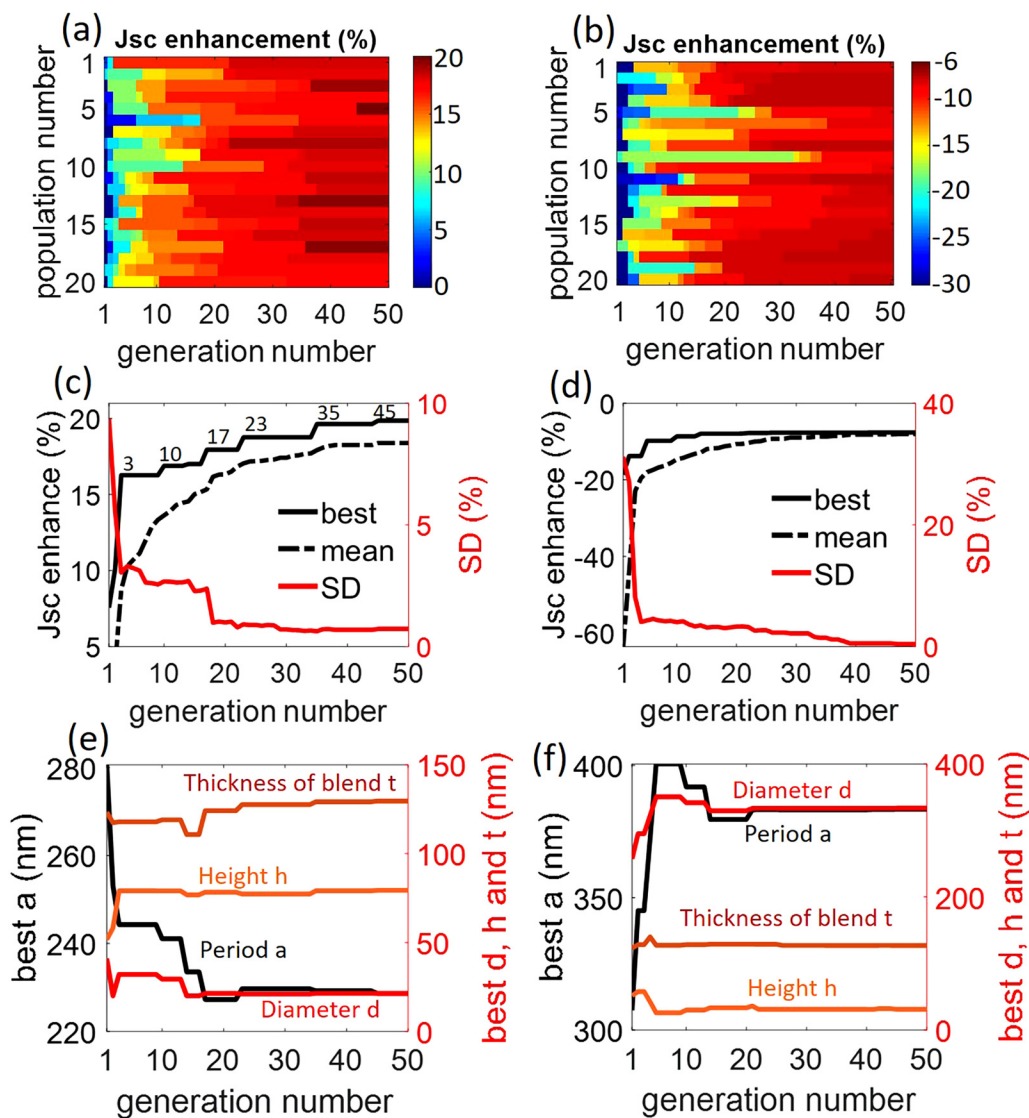
FIG. 2. J_{sc} enhancement of (a) nanoparticle array solar cells and (b) nanohole-array solar cells for all the populations and generations of the PSO. (c) and (d) display the best (black lines), mean (black dashed lines), and standard deviation (red lines) values of the J_{sc} enhancement as a function of the generation number of the PSO for particle array solar cells and hole array solar cells, respectively. The numbers on the line indicate the generations at which the best J_{sc} enhancement value of the populations evolves to a higher value. (e) and (f) show period a (black lines), diameter d (red lines), height h (pink lines), and thickness of the blend t (dark-red lines) of the best population as a function of the generation number for nanoparticle and nanohole-array solar cells, respectively.

absorptance in the blend of the nanoparticle device and the absorptance in the blend of the reference device. There are two clear peaks in the spectrum of the absorption enhancement, located on the absorption edges of the organic blend.

We have calculated the absorptance spectrum in the volume occupied by the Al nanoparticles to characterize the loss introduced by the plasmonic nanostructures. This absorptance, shown in Fig. 3(a) with the blue curve, is negligible compared to the absorption in the

blend. Furthermore, the absorptance spectra of the electrodes and transport materials are given in Fig. S2 of the supplementary material. The total reflectance and absorptance spectra of the solar cells are displayed in Fig. 3(b) with black and red curves, respectively, and for the nanoparticle array solar cell and the reference solar cell with solid and dashed curves, respectively.

To sort out the mechanism leading to the enhanced absorption of the nanoparticle array in the OSC, we investigate the electric-field
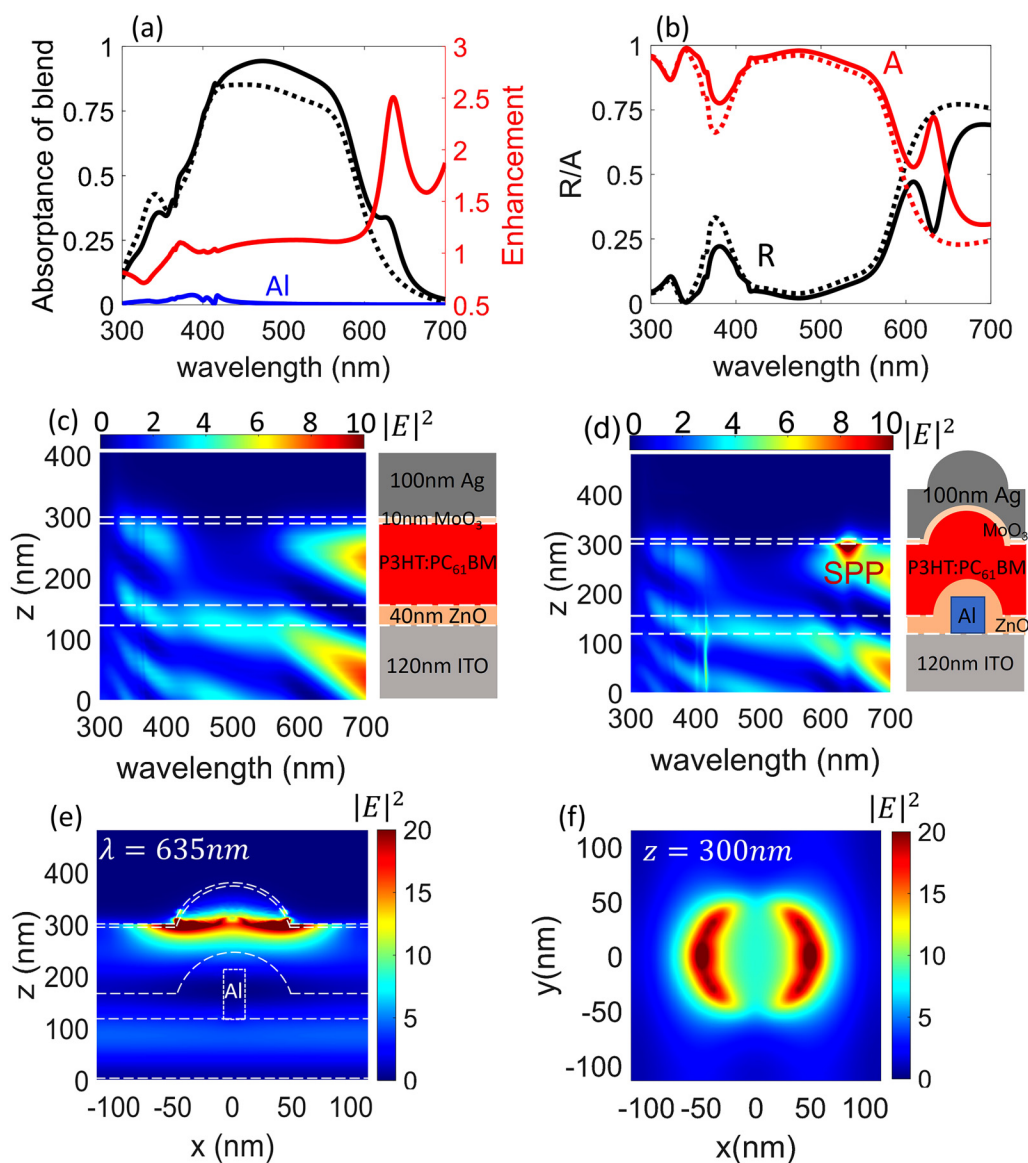
FIG. 3. (a) Absorptance spectra of the blend in the optimal nanoparticle array solar cell (black curve), in the reference solar cell with the same thickness of blend (dashed black curve), and the absorption enhancement (red curve). The absorptance in the Al nanoparticles is plotted as a blue curve. (b) Total reflection (black curves) and absorptance (red curves) of the optimal nanoparticle array solar cell (solid curves) and the reference solar cell (dashed curves). (c) and (d) are the electric-field intensity $|E|^2$ integrated in the xy-plane and in the wavelength range of 300–700 nm as a function of height for the reference solar cell and the optimal nanoparticle array solar cell, respectively. The dashed lines indicate the height of the different interfaces. The cross sections of the solar cells are schematically represented on the right panels of (c) and (d). Electric-field intensity distributions $|E|^2$ in the xz-plane (e) and the xy-plane (f) at 635 nm in a unit cell of the optimized nanoparticle array solar cell. The boundaries of the Al nanodisk and the device layers are indicated with the dashed white lines/curves in (e).

intensity integrated in the xy-plane as a function of position in the z-direction and the wavelength, as shown in Fig. 3(c) for the reference solar cell and in Fig. 3(d) for the nanoparticle solar cell. The field in the blend for the reference cell is mainly enhanced at $\simeq 340$ and $\simeq 700$ nm due to Fabry–Perot resonances in the planar structure. The resonant field enhancement at 700 nm does not contribute to the net solar cell absorption due to the low extinction coefficient of the blend at these wavelengths.

The resonant field enhancement due to the Fabry–Perot resonances in the nanoparticle solar cell is reduced compared to the
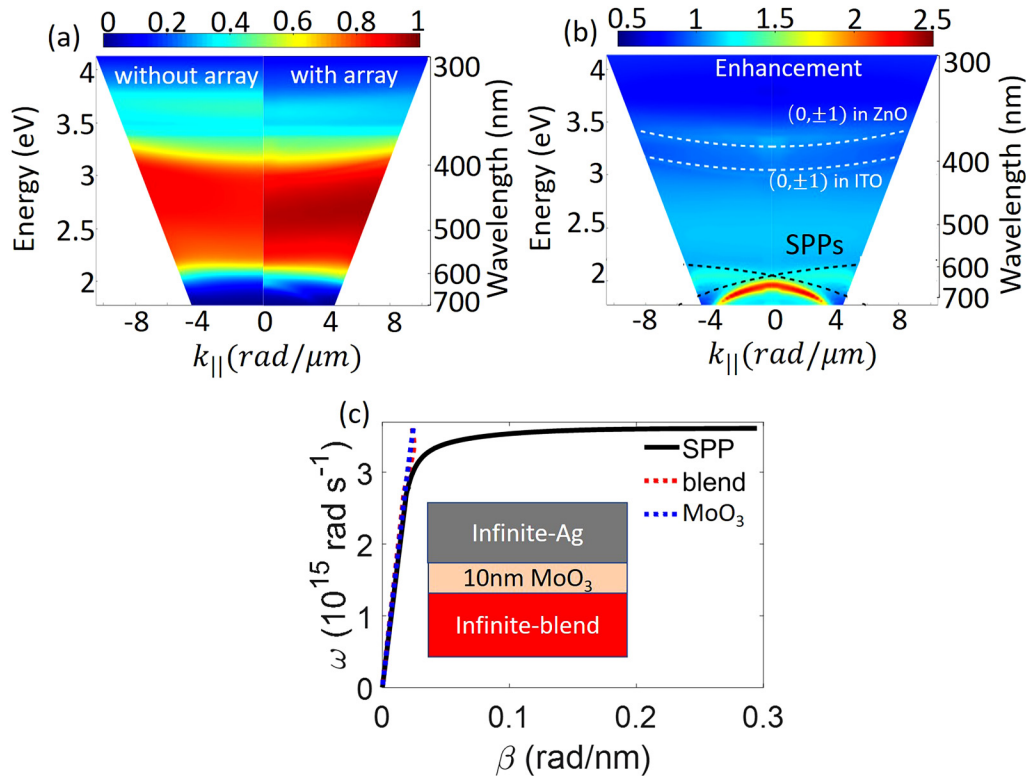
FIG. 4. (a) Absorptance dispersion of the organic blend in a reference solar cell (left) and in an optimal nanoparticle array solar cell (right). (b) Absorption enhancement of the organic blend for the nanoparticle solar cell. The dispersion of grating coupled SPPs and in-plane diffraction orders (Rayleigh anomalies) are indicated with black dotted and white dotted curves, respectively. (c) Dispersion relation of SPPs in an Ag/MoO$_3$/blend three-layer system with a MoO$_3$ thickness of 10 nm (black curve). The light cone of the organic blend (dashed red line) and MoO$_3$ (dashed blue line) are also plotted.

reference solar cell [see Fig. 3(d)]. However, a pronounced enhancement of the field close to the Ag anode-MoO$_3$ layer is apparent at 635 nm. This enhancement is also visible in the spatial distributions of the electric-field intensity in a unit cell at 635 nm for normal incidence, shown in Fig. 3(e) for the xz-plane across the middle of the particles and Fig. 3(f) for the xy-plane at the interface between Ag and MoO$_3$. We attribute this enhancement to the diffractive coupling of the incident light to surface plasmon polaritons (SPPs) at the Ag interface. This excitation of SPPs contributes to a 2.5-fold absorption enhancement in the blend. In addition, it results in absorption peaks in Ag and MoO$_3$, but a reduction of the absorption in ITO, as shown in Fig. S2 of the supplementary material. The SPP corresponds to a minimum of the reflectance and a peak of the total absorptance of the full device, as can be seen in Fig. 3(b).

To investigate the effect of the corrugation introduced by the nanoparticle array that is responsible for the diffractive coupling to SPPs and to exclude a possible effect of the nanoparticles, we have simulated a similar corrugated solar cell but without nanoparticles. These results are given in Sec. IV of the supplementary material, showing a similar enhancement of the absorptance in the OSC and of J_{sc}, albeit having slightly lower values. This result supports the

interpretation that the main mechanism leading to the increased absorption are SPPs at that Ag electrode. Nanoparticles are needed to form the periodic structure and corrugation that enables the diffractive coupling to SPPs. However, the material forming these nanoparticles is not as critical as could be initially expected. Further improvement in the absorption could be attained by considering periodic lattices with a higher rotational symmetry, such as hexagonal arrays.

V. OBLIQUE ANGLE ILLUMINATION

To investigate the dispersive response of the nanoparticle array solar cell, we have simulated the absorptance under oblique angle illumination. The absorptance dispersion diagrams for TM polarization are plotted in Fig. 4(a) for the reference solar cell (left panel) and the nanoparticle array solar cell (right panel). These dispersion diagrams represent the absorptance of the blend as a function of the photon energy/wavelength and the wave vector component of the incident wave parallel to the surface, i.e., $k_{\parallel} = (2\pi/\lambda)\sin(\theta)$, where θ is the angle of incidence. The dispersions are symmetric with respect to normal incidence ($k_{\parallel} = 0$); therefore, we only plot them for negative and positive angles, respectively, to facilitate their

comparison. As can be appreciated, the absorptance of the blend is enhanced in almost the entire angular dispersion, apart from the UV region where the Fabry–Perot resonance in the planar structure is reduced by the nanoparticles.

The dispersion absorption enhancement is plotted in Fig. 4(b). The main features in this figure are the enhancement peaks that, as we show next, follow the dispersion of SPPs. To determine the SPP dispersion, we first calculate the SPP wave number for a three-layer system, consisting of a semi-infinite Ag layer and blend, separated by a layer of 10 nm of MoO_3. The dispersion relation can be obtained by calculating the eigenstates of this three-layer system, given by

$$e^{-2k_1 l} = \frac{k_1/\varepsilon_1 + k_2/\varepsilon_2}{k_1/\varepsilon_1 - k_2/\varepsilon_2} \frac{k_1/\varepsilon_1 + k_3/\varepsilon_3}{k_1/\varepsilon_1 - k_3/\varepsilon_3} \qquad (4)$$

and

$$k_i^2 = \beta^2 - k_0^2 \varepsilon_i, \qquad (5)$$

with $i = 1, 2$ and 3 corresponding to MoO_3, Ag, and the blend, respectively, and $l = 10$ nm is the thickness of MoO_3. The dispersion of the SPP at the interface Ag–MoO_3/blend is displayed in Fig. 4(c). At low frequencies, the SPP dispersion (black curve) approaches the light cones of the blend (dashed red line) and of MoO_3 (dashed blue line). However, the incident plane wave onto the nanoparticle solar cell acquires an additional momentum by scattering with the periodic lattice, leading to the diffraction coupling condition into SPPs,

$$\boldsymbol{\beta} = \mathbf{k}_\parallel + \frac{2\pi}{a}(i\hat{u}_x, j\hat{u}_y), \qquad (6)$$

where (i, j) is the order of diffraction in the x- and y-directions and a is the period of a square array. Here, we focus on the in-plane $(1,0)$ and $(-1,0)$ diffraction orders from the array, defined by the polarization of the incident wave. The calculated SPPs dispersion is plotted with the dotted-black curve in Fig. 4(b). This dispersion follows the simulated dispersion bands of enhanced absorption, confirming that these bands result from the grating coupling of the incident wave to SPPs at the Ag interface.

We also see in Fig. 4(b) bands with a weaker absorption enhancement. These bands follow the dispersion of Rayleigh anomalies (RAs), i.e., in-plane diffracted orders, which can be calculated with the grating equation considering that the diffracted wave is on the plane of the array.[44] The white-dotted curves in Fig. 4(b) represent the calculation of these RAs for the degenerate $(0, \pm 1)$ diffraction orders. Considering that the nanoparticle array is placed on top of ITO and covered by the layer of ZnO and the organic blend, two RAs are apparent, corresponding to the upper and lower media. Both RAs slightly increase the absorption due to the diffraction of the incident wave in the plane of the array (see Sec. III in the supplementary material).

VI. CONCLUSIONS

To summarize, we have investigated the J_{sc} enhancement of organic solar cells with nanostructured electrodes formed by Al nanoparticle or nanohole squared arrays. By combining a particle

swarm optimization algorithm with 3D finite-difference time-domain simulations, the structural parameters of the arrays and the thickness of the organic blend layer have been optimized to maximize the J_{sc} enhancement of the solar cell. The optimal nanoparticle array solar cell reaches a remarkable 20% enhancement of J_{sc} compared to a standard planar solar cell, which is mediated by the grating coupling of the incident light into surface plasmon polaritons at the Ag electrode interface and in-plane diffraction orders. However, J_{sc} is reduced even for the optimum nanohole array due to the reduction of coupling of the incident light into the active blend of the organic solar cell. These findings reduce the applicability of nanohole arrays as semitransparent electrodes replacing ITO but highlight the potential improvement of organic solar cells with nanoparticle arrays on top of ITO.

VII. METHODS

Numerical simulations of the absorptance and short-circuit currents of different organic solar cells were carried out using a commercial FDTD software (Lumerical Solutions, Inc., 2022a and 2021R1.4). 3D-FDTD simulations were performed to calculate the absorbed power by the blend layer in OSCs. The raw $n(\omega)$ and $\kappa(\omega)$ data of P3HT:$PC_{61}BM$ were obtained from Ref. 21. Complex refractive indexes of Al, Ag, MoO_3, ITO, and ZnO were obtained from spectral ellipsometry. The optical constant of the glass substrate was set to 1.46. Before running the simulations, Lumerical uses a multi-coefficient model with a polynomial fit to the real and imaginary components of the experimental/raw complex refractive index in a specific wavelength range that is consistent with Kramers–Kronig relations.

The simulations of the organic solar cells based on nanostructured electrodes were performed using Bloch periodic boundary conditions in the x- and y-directions that define the size of the unit cell of the periodic arrays and perfectly matched layer (PML) boundaries in the z-direction at a distance of five times the longest simulated wavelength. The particle or hole arrays were positioned in the middle plane. The illumination consists of a broadband beam, approximated by a plane wave with TM-polarization, which is incident normal or oblique to the array plane (the xy-plane) from the glass substrate. Non-uniform meshes are used, and a set of $dx = dy = 2$ and $dz = 1$ nm refinement mesh is used in the array layer and corrugated conformal interfaces, extending over a distance of 10 nm from the edges of the nanoparticle/nanohole. Long simulation times (6000 fs) with auto-shut off levels of 10^{-6} were used to ensure the convergence of the simulations. To extract the absorptance of the blend layer, an analysis group that measures the spatial absorption profile was created. This group includes a 3D-field monitor to extract the spatial near-field amplitude and a 3D-index monitor to retrieve the spatial refractive index data. These two monitors should have the same grid points in the same volume. An analysis script was edited in the analysis group to calculate the fraction of the power from the source that is absorbed within the volume using Eq. (1). Another script file was created to calculate the power absorbed in a region where the refractive index is that of a particular material (organic blend, Al, ITO, ZnO, MoO_3, or Ag) for all frequencies by integrating the absorption over this material. The 3D-field monitor in the above analysis group can

also be used to calculate the electric-field intensity by integrating the fields in the xy-plane for different z positions.

To calculate the short-circuit current of the organic solar cells, a volume analysis was created in the simulations with a 3D-field and index monitors where the organic blend was placed. An analysis script was edited to calculate the number of absorbed photons by the organic blend per unit volume, which was assumed equal to the number of generated electron/hole pairs (photon generate rate). The short-circuit current is obtained by dividing the source intensity, which is normalized to match the standard AM1.5 solar power spectrum.

A homemade PSO code was edited in a Lumerical script to optimize the structural parameters of the plasmonic nanostructured electrodes yielding the highest J_{sc}. To begin the optimization, the algorithm was initialized with 20 Al nanoparticle-/nanohole-array OSCs with random parameters, which were simulated using Lumerical to obtain the J_{sc}. The computed J_{sc} values were evaluated with the PSO algorithm, producing a new set of parameters for the next generation that was simulated with Lumerical. This iteration was repeated until 50 generations were performed.

SUPPLEMENTARY MATERIAL

See the supplementary material that includes complex refractive indexes of the different materials forming the organic solar cells that were used for the optimization and simulations, absorption spectra of each material for the reference solar cell and the nanoparticle solar cell with maximum J_{sc}, localized surface plasmon (LSP) resonance of a single nanoparticle embedded into a solar cell environment, and the effect on the absorptance of removing the nanoparticles but retaining the corrugation of the solar cell.

ACKNOWLEDGMENTS

AUTHOR DECLARATIONS

Conflict of Interest

The authors have no conflicts to disclose.

Author Contributions

Ping Bai: Conceptualization (equal); Data curation (equal); Formal analysis (equal); Investigation (equal); Methodology (equal); Resources (equal); Software (equal); Validation (equal); Visualization (equal); Writing – original draft (equal); Writing – review & editing (equal). **Mohamed S. Abdelkhalik:** Validation (equal). **Diogo G. A. Castanheira:** Validation (equal). **Jaime Gómez Rivas:** Funding acquisition (equal); Investigation (equal); Project administration (equal); Supervision (equal); Validation (equal); Writing – review & editing (equal).

DATA AVAILABILITY

The data that support the findings of this study are available from the corresponding author upon reasonable request.

REFERENCES

[1]M. C. Scharber and N. S. Sariciftci, "Efficiency of bulk-heterojunction organic solar cells," Prog. Polym. Sci. **38**, 1929–1940 (2013).

[2]H. Hoppe and N. S. Sariciftci, "Organic solar cells: An overview," J. Mater. Res. **19**, 1924–1945 (2004).

[3]A. Uddin, "Organic solar cells," in *Comprehensive Guide on Organic and Inorganic Solar Cells* (Elsevier, 2022), pp. 25–55.

[4]H. Lee, C. Park, D. H. Sin, J. H. Park, and K. Cho, "Recent advances in morphology optimization for organic photovoltaics," Adv. Mater. **30**, 1800453 (2018).

[5]P. E. Shaw, A. Ruseckas, and I. D. W. Samuel, "Exciton diffusion measurements in poly(3-hexylthiophene)," Adv. Mater. **20**, 3516–3520 (2008).

[6]A. J. Moulé, J. B. Bonekamp, and K. Meerholz, "The effect of active layer thickness and composition on the performance of bulk-heterojunction solar cells," J. Appl. Phys. **100**, 94503 (2006).

[7]F. Cheng, G. Fang, X. Fan, N. Liu, N. Sun, P. Qin, Q. Zheng, J. Wan, and X. Zhao, "Enhancing the short-circuit current and efficiency of organic solar cells using MoO_3 and CuPc as buffer layers," Sol. Energy Mater. Sol. Cells **95**, 2914–2919 (2011).

[8]F. Li, L. Kou, W. Chen, C. Wu, and T. Guo, "Enhancing the short-circuit current and power conversion efficiency of polymer solar cells with graphene quantum dots derived from double-walled carbon nanotubes," NPG Asia Mater. **5**, e60 (2013).

[9]H.-Y. Chen, J. Hou, S. Zhang, Y. Liang, G. Yang, Y. Yang, L. Yu, Y. Wu, and G. Li, "Polymer solar cells with enhanced open-circuit voltage and efficiency," Nat. Photonics **3**, 649–653 (2009).

[10]D. Di Nuzzo, G.-J. A. Wetzelaer, R. K. Bouwer, V. S. Gevaerts, S. C. Meskers, J. C. Hummelen, P. W. Blom, and R. A. Janssen, "Simultaneous open-circuit voltage enhancement and short-circuit current loss in polymer: Fullerene solar cells correlated by reduced quantum efficiency for photoinduced electron transfer," Adv. Energy Mater. **3**, 85–94 (2013).

[11]N. K. Elumalai and A. Uddin, "Open circuit voltage of organic solar cells: An in-depth review," Energy Environ. Sci. **9**, 391–410 (2016).

[12]J. Yuan, Y. Zhang, L. Zhou, G. Zhang, H.-L. Yip, T.-K. Lau, X. Lu, C. Zhu, H. Peng, P. A. Johnson, and M. Leclerc, "Single-junction organic solar cell with over 15% efficiency using fused-ring acceptor with electron-deficient core," Joule **3**, 1140–1151 (2019).

[13]A. Raman, Z. Yu, and S. Fan, "Dielectric nanostructures for broadband light trapping in organic solar cells," Opt. Express **19**, 19015–19026 (2011).

[14]H.-P. Wang, D.-H. Lien, M.-L. Tsai, C.-A. Lin, H.-C. Chang, K.-Y. Lai, and J.-H. He, "Photon management in nanostructured solar cells," J. Mater. Chem. C **2**, 3144–3171 (2014).

[15]B. Lipovšek, A. Čampa, F. Guo, C. J. Brabec, K. Forberich, J. Krč, and M. Topič, "Detailed optical modelling and light-management of thin-film organic solar cells with consideration of small-area effects," Opt. Express **25**, A176–A190 (2017).

[16]J.-L. Wu, F.-C. Chen, Y.-S. Hsiao, F.-C. Chien, P. Chen, C.-H. Kuo, M. H. Huang, and C.-S. Hsu, "Surface plasmonic effects of metallic nanoparticles on the performance of polymer bulk heterojunction solar cells," ACS Nano **5**, 959–967 (2011).

[17]L. Qiao, D. Wang, L. Zuo, Y. Ye, J. Qian, H. Chen, and S. He, "Localized surface plasmon resonance enhanced organic solar cell with gold nanospheres," Appl. Energy **88**, 848–852 (2011).

[18]N. C. Lindquist, W. A. Luhman, S.-H. Oh, and R. J. Holmes, "Plasmonic nanocavity arrays for enhanced efficiency in organic photovoltaic cells," Appl. Phys. Lett. **93**, 350 (2008).

[19]W. J. Dong, H. K. Yu, and J.-L. Lee, "Abnormal dewetting of Ag layer on three-dimensional ITO branches to form spatial plasmonic nanoparticles for organic solar cells," Sci. Rep. 10, 12819 (2020).

[20]K. Yao, H. Zhong, Z. Liu, M. Xiong, S. Leng, J. Zhang, Y.-X. Xu, W. Wang, L. Zhou, H. Huang, and A. K. Y. Jen, "Plasmonic metal nanoparticles with core–bishell structure for high-performance organic and perovskite solar cells," ACS Nano 13, 5397–5409 (2019).

[21]C. Stelling, C. R. Singh, M. Karg, T. A. König, M. Thelakkat, and M. Retsch, "Plasmonic nanomeshes: Their ambivalent role as transparent electrodes in organic solar cells," Sci. Rep. 7, 42530 (2017).

[22]H. Shen, P. Bienstman, and B. Maes, "Plasmonic absorption enhancement in organic solar cells with thin active layers," J. Appl. Phys. 106, 073109 (2009).

[23]J. R. Tumbleston, D.-H. Ko, E. T. Samulski, and R. Lopez, "Absorption and quasiguided mode analysis of organic solar cells with photonic crystal photoactive layers," Opt. Express 17, 7670–7681 (2009).

[24]D. H. Wang, K. H. Park, J. H. Seo, J. Seifter, J. H. Jeon, J. K. Kim, J. H. Park, O. O. Park, and A. J. Heeger, "Enhanced power conversion efficiency in PCDTBT/PC$_{70}$BM bulk heterojunction photovoltaic devices with embedded silver nanoparticle clusters," Adv. Energy Mater. 1, 766–770 (2011).

[25]X. Li, W. C. H. Choy, H. Lu, W. E. Sha, and A. H. P. Ho, "Efficiency enhancement of organic solar cells by using shape-dependent broadband plasmonic absorption in metallic nanoparticles," Adv. Funct. Mater. 23, 2728–2735 (2013).

[26]L. Lu, Z. Luo, T. Xu, and L. Yu, "Cooperative plasmonic effect of Ag and Au nanoparticles on enhancing performance of polymer solar cells," Nano Lett. 13, 59–64 (2013).

[27]J. Zhu, M. Xue, H. Shen, Z. Wu, S. Kim, J.-J. Ho, A. Hassani-Afshar, B. Zeng, and K. L. Wang, "Plasmonic effects for light concentration in organic photovoltaic thin films induced by hexagonal periodic metallic nanospheres," Appl. Phys. Lett. 98, 151110 (2011).

[28]J. van de Groep, D. Gupta, M. A. Verschuuren, M. M. Wienk, R. A. Janssen, and A. Polman, "Large-area soft-imprinted nanowire networks as light trapping transparent conductors," Sci. Rep. 5, 11414 (2015).

[29]Q. G. Du, H. Ren, L. Wu, P. Bai, C. E. Png, X. W. Sun, C. H. Kam, and C. M. de Sterke, "Light absorption mechanism in organic solar cells with hexagonal lattice nanohole aluminum transparent electrodes," J. Opt. 17, 085901 (2015).

[30]J. Robinson and Y. Rahmat-Samii, "Particle swarm optimization in electromagnetics," IEEE Trans. Antennas Propag. 52, 397–407 (2004).

[31]C. Forestiere, M. Donelli, G. F. Walsh, E. Zeni, G. Miano, and L. Dal Negro, "Particle-swarm optimization of broadband nanoplasmonic arrays," Opt. Lett. 35, 133–135 (2010).

[32]M. Notarianni, K. Vernon, A. Chou, M. Aljada, J. Liu, and N. Motta, "Plasmonic effect of gold nanoparticles in organic solar cells," Sol. Energy 106, 23–37 (2014).

[33]C. C. Wang, W. C. Choy, C. Duan, D. D. Fung, E. Wei, F.-X. Xie, F. Huang, and Y. Cao, "Optical and electrical effects of gold nanoparticles in the active layer of polymer solar cells," J. Mater. Chem. 22, 1206–1211 (2012).

[34]B. Wu, X. Wu, C. Guan, K. Fai Tai, E. K. L. Yeow, H. Jin Fan, N. Mathews, and T. C. Sum, "Uncovering loss mechanisms in silver nanoparticle-blended plasmonic organic solar cells," Nat. Commun. 4, 2004 (2013).

[35]N. Kalfagiannis, P. Karagiannidis, C. Pitsalidis, N. Panagiotopoulos, C. Gravalidis, S. Kassavetis, P. Patsalas, and S. Logothetidis, "Plasmonic silver nanoparticles for improved organic solar cells," Sol. Energy Mater. Sol. Cells 104, 165–174 (2012).

[36]M. Xue, L. Li, B. J. Tremolet de Villers, H. Shen, J. Zhu, Z. Yu, A. Z. Stieg, Q. Pei, B. J. Schwartz, and K. L. Wang, "Charge-carrier dynamics in hybrid plasmonic organic solar cells with Ag nanoparticles," Appl. Phys. Lett. 98, 119 (2011).

[37]V. Kochergin, L. Neely, C.-Y. Jao, and H. D. Robinson, "Aluminum plasmonic nanostructures for improved absorption in organic photovoltaic devices," Appl. Phys. Lett. 98, 73 (2011).

[38]M. Sygletou, G. Kakavelakis, B. Paci, A. Generosi, E. Kymakis, and E. Stratakis, "Enhanced stability of aluminum nanoparticle-doped organic solar cells," ACS Appl. Mater. Interfaces 7, 17756–17764 (2015).

[39]S. Vedraine, P. Torchio, D. Duché, F. Flory, J.-J. Simon, J. Le Rouzo, and L. Escoubas, "Intrinsic absorption of plasmonic structures for organic solar cells," Sol. Energy Mater. Sol. Cells 95, S57–S64 (2011).

[40]P. T. Dang, T. K. Nguyen, and K. Q. Le, "Revisited design optimization of metallic gratings for plasmonic light-trapping enhancement in thin organic solar cells," Opt. Commun. 382, 241–245 (2017).

[41]M. Kaya and S. Hajimirza, "Application of artificial neural network for accelerated optimization of ultra thin organic solar cells," Sol. Energy 165, 159–166 (2018).

[42]P. Bai, S. Ter Huurne, E. van Heijst, S. Murai, and J. Gómez Rivas, "Evolutionary optimization of light-matter coupling in open plasmonic cavities," J. Chem. Phys. 154, 134110 (2021).

[43]T. W. Ebbesen, H. J. Lezec, H. Ghaemi, T. Thio, and P. A. Wolff, "Extraordinary optical transmission through sub-wavelength hole arrays," Nature 391, 667–669 (1998).

[44]R. W. Wood, "XLII. On a remarkable case of uneven distribution of light in a diffraction grating spectrum," Lond. Edinb. Dubl. Philos. Mag. J. Sci. 4, 396–402 (1902).